JOURNAL OF THERMOPHYSICS AND HEAT TRANSFER
Vol. 8, No. 4, Oct.–Dec. 1994

Finite Element Analysis of Low-Speed Compressible Flows Within Convectively Cooled Structures

Phillip W. Yarrington*
Lockheed Engineering and Sciences Company, Inc., Hampton, Virginia 23666
and
Earl A. Thornton†
University of Virginia, Charlottesville, Virginia 22903

A Galerkin-based finite element algorithm is used to solve the transient compressible Navier-Stokes equations for low-speed flows within convectively cooled structures. This algorithm solves simultaneously for the temperature distribution in the structure and coolant. While most flows for which the algorithm is intended have low Mach numbers, the compressible equations are used to represent gradients of density and other flow quantities that accompany significant temperature variations. The algorithm is first applied to flows with small Mach numbers with little or no temperature variation for validation against incompressible flow solutions. The algorithm is then used to analyze an experimental model of a convectively cooled structure.

Nomenclature

A = element area
$\boldsymbol{BT}$ = boundary term vector
c = specific heat
D_h = hydraulic diameter
E, F = fluxes
E_t = total energy
e = internal energy
$\boldsymbol{F}$ = global/element residual vectors
h = channel height
J = global Jacobian matrix
K, L, M = element matrices
k = thermal conductivity
M = Mach number
N = element interpolation functions
Nu = Nusselt number
n = direction cosines
$\boldsymbol{n}$ = normal vector
P = static pressure
Pr = Prandtl number
q = heat flux
$\boldsymbol{R}$ = element vector
Re = Reynolds number
r = number of nodes in an element
S = plate length
T = static temperature
t = time
U = conservation variable or average velocity
u, v = velocity components in the x and y directions
$\boldsymbol{V}$ = velocity vector
W = weighting function
X_r = reattachment length
x, y = Cartesian coordinates
Γ = domain boundary
$\boldsymbol{\Delta U}$ = change in conservation variable between iterations
μ = viscosity
ρ = density
σ = normal stresses
τ = shear stresses
Ω = solution domain

Subscripts
f = fluid quantity
I = inviscid quantity
k = iteration level
m = mean quantity
n = normal quantity
s = solid quantity or surface quantity
V = viscous quantity
v = constant volume
w = wall quantity
∞ = freestream condition

Superscripts
(e) = element quantity
n = time level
$+$ = nondimensional quantity

Introduction

CONVECTIVELY cooled structures have become strong candidates for dealing with the sustained severe thermal environments that are expected for high-speed flight vehicles such as the National Aero-Space Plane (NASP). Research conducted on convectively cooled structures in the 1960s and 1970s is reviewed in Ref. 1. While the complex external flows that are generated on hypersonic vehicles are topics of current active research,[2] relatively little research has been done on the coolant flows required for structures to survive such an environment.

A typical cross section of a convectively cooled structure is shown in Fig. 1. In this example, an aerodynamic skin and coolant passage protect a primary aircraft structure from aerodynamic heating. The skin transfers the heat generated by the aerothermal loading to a low-temperature coolant flow. In the NASP engine structure, a proposed coolant is the cryogenic hydrogen later used as propulsion system fuel. Accurate prediction of temperatures in the aircraft skin is important in the design and analysis procedure because severe localized heating has been shown to cause significant inelastic structural deformations.[3] An analysis procedure is therefore necessary to predict skin temperatures and heat transfer characteristics of the coolant flow.

Received Oct. 25, 1993; revision received March 1, 1994; accepted for publication March 4, 1994.

*Senior Associate Engineer.
†Professor of Aerospace Engineering and Director, Center for Light Thermal Structures. Associate Fellow AIAA.

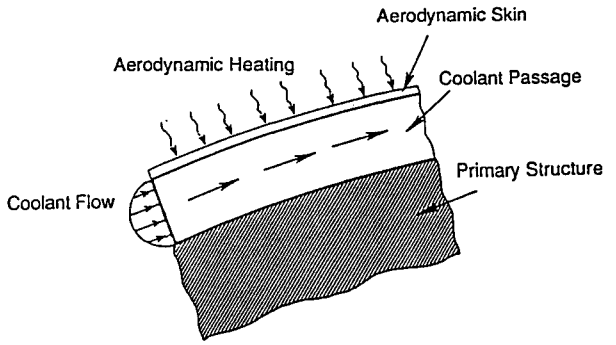

Fig. 1 Convectively cooled structure typical cross section.

There are basically two representations of this type of heat transfer available. For the first of these, called the engineering approach, a detailed resolution of the temperature and flowfield are not obtained. A finite element methodology for the engineering approach was developed and applied in Ref. 4. The engineering approach has the advantage of giving good overall temperature results and heat transfer characteristics while being computationally nonintensive. It does not, however, provide detailed temperature solutions in areas of intense local heating. This lack of detail leads to a second representation of heat transfer called the continuum approach.

The continuum approach models the combined conduction/convection heat transfer of the flow and structure using the partial differential equations governing the conservation of mass, momentum, and energy. The complexities involved in the solution of the continuum problem have led to the use of numerical methods to approximate the differential conservation equations with algebraic equations.

Problems involving internal laminar forced convection have been widely studied. An extensive review of analytical and computational solutions to problems of this nature can be found in Ref. 5. Typically, solution methods for problems involving laminar convection have attempted to solve the fluid and solid governing equations separately. Even in cases where the fluid and solid heat transfer equations are solved together, the assumptions of fluid incompressibility and constant properties are usually made to simplify the analysis. For example, Scotti[6] recently studied convective cooling for a locally heated skin using an incompressible finite difference model. To uncouple the mass and momentum equations from the energy equation, the properties of the fluid were assumed to be constant. Scotti noted that this assumption might lead to inaccurate results, especially for compressible fluids such as hydrogen undergoing large local temperature changes. For this reason, a coolant such as hydrogen subjected to substantial temperature gradients should be modeled as compressible due to local variations of density in the heated area. Solutions for low-speed compressible flow are rare, however. One notable exception is the recent work of Wood and Carlisle[7] who considered the combined problem of flow and heat transfer in a model of a leading-edge coolant system. Their analysis used a finite difference approximation to the governing equations and included variable thermodynamic properties for the hydrogen coolant and coupling of the energy equation with the mass and momentum equations.

The present work has been motivated by some recent flux-based finite element schemes[8-10] that have been successfully applied to problems involving high-speed compressible flow, heat transfer, and thermal-structural interaction. These schemes all employ the governing equations in conservation form. The purpose of this article is to present a finite element algorithm used to solve the combined convection/conduction problem for low-speed flows within convectively cooled structures. The definition of a low-speed flow used in the present context is one for which the Mach number is less than about 0.3.

Problem Formulation

Laminar Compressible Flow

The partial differential equations governing laminar compressible flow are derived from the conservation of mass, momentum, and energy. These equations can be expressed in flux-conservation form as

$$\frac{\partial}{\partial t}\{U\} + \frac{\partial}{\partial x}\{E_I - E_V\} + \frac{\partial}{\partial y}\{F_I - F_V\} = 0 \tag{1}$$

In Eq. (1), $\{U\}$ represents the conservation variables, $\{E_I\}$ and $\{F_I\}$ represent the inviscid fluxes, and $\{E_V\}$ and $\{F_V\}$ represent the viscous fluxes. These quantities can be expressed in vector form as

$$\begin{aligned}
\{U\} &= \{\rho \quad \rho u \quad \rho v \quad \rho E_t\}^T \\
\{E_I\} &= \{\rho u \quad \rho uu \quad \rho uv \quad (\rho E_t + P)u\}^T \\
\{F_I\} &= \{\rho v \quad \rho uv \quad \rho vv \quad (\rho E_t + P)v\}^T \\
\{E_V\} &= \{0 \quad \sigma_{xx} - P \quad \tau_{yx} \quad (u\sigma_{xx} + v\tau_{yx} - q_x)\}^T \\
\{F_V\} &= \{0 \quad \tau_{xy} \quad \sigma_{yy} - P \quad (u\tau_{xy} + v\sigma_{yy} - q_y)\}^T
\end{aligned} \tag{2}$$

where P is the static pressure that is a function of density and temperature. The viscous stresses σ_{xx}, τ_{xy}, τ_{yx}, and σ_{yy} are expressed as

$$\begin{aligned}
\sigma_{xx} &= \frac{2}{3}\mu\left[2\frac{\partial u}{\partial x} - \frac{\partial v}{\partial y}\right] \qquad \sigma_{yy} = \frac{2}{3}\mu\left[-\frac{\partial u}{\partial x} + 2\frac{\partial v}{\partial y}\right] \\
\tau_{xy} &= \tau_{yx} = \mu\left[\frac{\partial u}{\partial y} + \frac{\partial v}{\partial x}\right]
\end{aligned} \tag{3}$$

where μ denotes the viscosity, a function of temperature. The heat fluxes q_x and q_y can be expressed as

$$q_x = -k_f\frac{\partial T}{\partial x} \qquad q_y = -k_f\frac{\partial T}{\partial y} \tag{4}$$

where k_f is the thermal conductivity of the fluid, also a function of temperature.

Equation (1) must be solved subject to appropriate initial and boundary conditions. The initial conditions consist of specifying the spatial distributions of the conservation variables at some initial time. Some typical boundary conditions include 1) inflow, 2) outflow, 3) slip wall, and 4) no-slip isothermal or adiabatic wall. The boundary conditions on the flow equations will be discussed in more detail in the section on numerical boundary conditions.

Solid Heat Conduction

The scalar equation governing heat conduction in a solid is based on the conservation of energy and can be written in a form similar to the fluid equations

$$\rho_s c_s\frac{\partial U}{\partial t} + \frac{\partial E}{\partial x} + \frac{\partial F}{\partial y} = 0 \tag{5}$$

where for solid heat conduction

$$U = T_s \qquad E = q_x \qquad F = q_y \tag{6}$$

In Eqs. (5) and (6), ρ_s is the density of the solid, c_s is the specific heat of the solid, T_s is the temperature of the solid,

and q_x and q_y are the heat fluxes in the x and y directions, respectively, given by

$$q_x = -k_s \frac{\partial T}{\partial x} \qquad q_y = -k_s \frac{\partial T}{\partial y} \tag{7}$$

where k_s is the thermal conductivity of an isotropic solid that is, in general, a function of temperature.

Boundary conditions for Eq. (5) consist of specifying the temperature on one part of the boundary while specifying the normal heat flux on the remainder of the boundary.

Conditions at Flow-Solid Interface

At a wall separating fluid and solid regions, the velocity of the flow is zero, and the only heat transfer mechanism between the fluid and solid is governed by Fourier's law:

$$q_n = -k \frac{\partial T}{\partial n} \tag{8}$$

An energy balance around the interface reveals that the energy leaving one surface must enter the other, so that $(q_n)_s + (q_n)_f = 0$. Also, the temperature at the fluid-solid interface must be continuous. This condition can be written $T_s = T_f$. These two conditions must be satisfied at each point along the fluid-solid interface. The interface between a fluid region and a solid region is complicated by the fact that the principle unknown quantity in the solid region is the solid temperature T_s, whereas the temperature in the fluid region T_f is a quantity that must be computed from the conservation variables, ρ, ρu, ρv, and ρE_t.

Solution Algorithm

Typical Conservation Equation

For simplicity, the finite element equations will be developed for a scalar conservation law of the form

$$\frac{\partial U}{\partial t} + \frac{\partial}{\partial x}(E_I - E_V) + \frac{\partial}{\partial y}(F_I - F_V) = 0 \tag{9}$$

where E_I and F_I are inviscid fluxes, E_V and F_V are viscous fluxes, and U is a conservation variable. The extension of the discretization from this scalar equation to the set of Eqs. (1) and (5) is straightforward. The first step in discretization is to multiply Eq. (9) by W and integrate over Ω. The viscous terms are then integrated by parts to obtain

$$\int_\Omega W\left(\frac{\partial U}{\partial t} + \frac{\partial E_I}{\partial x} + \frac{\partial F_I}{\partial \mathrm{d}y}\right) \mathrm{d}\Omega + \int_\Omega \left(\frac{\partial W}{\partial x} E_V + \frac{\partial W}{\partial y} F_V\right) \mathrm{d}\Omega - \int_\Gamma W\,(E_V n_x + F_V n_y)\,\mathrm{d}\Gamma = 0 \tag{10}$$

where n_x and n_y are the direction cosines of a vector normal to Γ. The boundary integral portion of Eq. (10) is used to prescribe the "natural" boundary condition in the analysis such as the static pressure on the momentum equation or the boundary heat flux on the energy equation. The next step is to interpolate the conservation variables as well as the inviscid and viscous fluxes over each element in terms of nodal values of these quantities

$$U(x, y, t)^{(e)} = \lfloor N(x, y)\rfloor\{U(t)\} \tag{11}$$

with similar expressions for $E(x, y, t)^{(e)}$ and $F(x, y, t)^{(e)}$, where $\lfloor N(x, y)\rfloor$ represents the element interpolation functions. After substituting Eq. (11) into Eq. (10) and replacing W with N, the following element equations are obtained:

$$[M]\left\{\frac{\mathrm{d}\boldsymbol{U}}{\mathrm{d}t}\right\} + [L_x]\{\boldsymbol{E}_I\} + [L_y]\{\boldsymbol{F}_I\} + [K_x]\{\boldsymbol{E}_V\} + [K_y]\{\boldsymbol{F}_V\} - \{\boldsymbol{BT}\} = 0 \tag{12}$$

where the element matrices are given by

$$[M] = \int_{\Omega^{(e)}} \{N\}\lfloor N\rfloor\,\mathrm{d}\Omega$$

$$[L_x] = \int_{\Omega^{(e)}} \{N\}\left\lfloor\frac{\partial N}{\partial x}\right\rfloor \mathrm{d}\Omega \quad [L_y] = \int_{\Omega^{(e)}} \{N\}\left\lfloor\frac{\partial N}{\partial y}\right\rfloor \mathrm{d}\Omega \tag{13}$$

$$[K_x] = \int_{\Omega^{(e)}} \left\{\frac{\partial N}{\partial x}\right\}\lfloor N\rfloor\,\mathrm{d}\Omega \quad [K_y] = \int_{\Omega^{(e)}} \left\{\frac{\partial N}{\partial y}\right\}\lfloor N\rfloor\,\mathrm{d}\Omega$$

$$\{\boldsymbol{BT}\} = \int_{\Gamma^{(e)}} \{N\}(E_V n_x + F_V n_y)\,\mathrm{d}\Gamma$$

The transient term, $\{\mathrm{d}U/\mathrm{d}t\}$, is evaluated at some time level $t + \theta\Delta t$ using a classical "time-marching" algorithm based upon finite difference methods.[11] The following approximation is introduced:

$$\left\{\frac{\mathrm{d}\boldsymbol{U}}{\mathrm{d}t}\right\}^{n+\theta} \approx \frac{\{\boldsymbol{U}\}^{n+1} - \{\boldsymbol{U}\}^n}{\Delta t} \tag{14}$$

where the superscripts n and $n + 1$ refer to the time level. The nodal quantities are evaluated at the $n + \theta$ time level as

$$\{\boldsymbol{U}\}^{n+\theta} = (1 - \theta)\{\boldsymbol{U}\}^n + \theta\{\boldsymbol{U}\}^{n+1} \tag{15}$$

Substituting Eqs. (14) and (15) into Eq. (12) gives

$$(1/\Delta t)[M]\{\boldsymbol{U}\}^{n+1} + \theta\{\boldsymbol{R}\}^{n+1} = (1/\Delta t)[M]\{\boldsymbol{U}\}^n - (1 - \theta)\{\boldsymbol{R}\}^n \tag{16}$$

where

$$\{\boldsymbol{R}\}^n = [L_x]\{\boldsymbol{E}_I\}^n + [L_y]\{\boldsymbol{F}_I\}^n + [K_x]\{\boldsymbol{E}_V\}^n + [K_y]\{\boldsymbol{F}_V\}^n - \{\boldsymbol{BT}\}^n \tag{17}$$

Equation (16) is the discretized form of Eq. (9) over a single element. It is assembled into a global system of equations using the standard finite element assembly procedure. For $\theta = 0$, the scheme is explicit, whereas for $\theta \neq 0$, it is implicit. This nonlinear system must be solved for $\{U\}^{n+1}$ at each time step. This is accomplished by linearizing Eq. (16) using Newton-Raphson (N-R) iterations. First, an element residual vector is established for each element

$$\{\boldsymbol{F}\}^{(e)} = (1/\Delta t)[M][\{\boldsymbol{U}\}^{n+1} - \{\boldsymbol{U}\}^n] + (1 - \theta)\{\boldsymbol{R}\}^n + \theta\{\boldsymbol{R}\}^{n+1} \tag{18}$$

The element residual vector $\{\boldsymbol{F}\}^{(e)}$ is assembled into a global residual vector, $\{\boldsymbol{F}\}$. To solve the system of equations created by assembling Eq. (16), the global vector $\{\boldsymbol{F}\}$ must be forced to $\{\boldsymbol{0}\}$. The N-R algorithm used to accomplish this is obtained by performing a Taylor expansion on each member of the global residual vector F_i

$$F_i(U_1 + \Delta U_1, \ldots, U_r + \Delta U_r) = F_i(U_1, \ldots, U_r) + \sum_{j=1}^{r} \frac{\partial F_i}{\partial U_j}\Delta U_j + O[(\Delta U)^2] \tag{19}$$

where r is the number of nodes in the global domain. The U_j in Eq. (19) are all unknowns and are the values of the conservation variable evaluated at the $n + 1$ time level. To obtain an iterative procedure, the left side of Eq. (19) is set equal to zero, the higher-order terms are neglected and Eq. (19) reduces to

$$\sum_{j=1}^{n} \frac{\partial F_i}{\partial U_j} \Delta U_j = -F_i(U_1, \ldots, U_n) \tag{20}$$

Equation (20) can be written in matrix form by setting $J_{ij} = \partial F_i/\partial U_j$:

$$[J]\{\Delta U\} = -\{F\} \tag{21}$$

The vector $\{\Delta U\}$ is the change in $\{U\}^{n+1}$ from one Newton iteration to the next. While the N-R method is presented here for a global system of equations, J and residual vector can be computed on an element basis and assembled into a global Jacobian matrix and global residual vector in the standard way. After Eq. (21) is solved for $\{\Delta U\}$, the solution to Eq. (16), $\{U\}^{n+1}$ is found by

$$\{U\}_{k+1}^{n+1} = \{U\}_k^{n+1} + \{\Delta U\}_k^{n+1} \tag{22}$$

where the subscript k indicates the number of the Newton iterate.

Once the nodal values of the conservation variables have been determined using Eq. (22), the nodal primitive variables and fluxes are then calculated using the conservation variable and flux definitions in Eq. (2). For example, $U_1 = \rho$, $U_2 = \rho u$, therefore the primitive variable u is calculated to be $u = U_2/U_1$.

Numerical Initial and Boundary Conditions

The fluid and solid conservation equations are solved subject to appropriate initial and boundary conditions. The initial conditions consist of specifying the distribution of the conservation variables $\{U\}$ at time zero. The following boundary conditions have been successfully applied to the fluid conservation of mass, momentum, and energy equations.

Supersonic Inflow

All conservation variables are specified on the inflow plane.

Subsonic Inflow

The inlet conditions depend on downstream conditions, therefore in the present work, ρ, ρu, and ρv are specified on the inflow plane. The conservation variable ρE_t is left unspecified.

Supersonic Outflow

All flow quantities are unspecified and are treated as natural boundary conditions.

Subsonic Outflow

The fluid is affected by the conditions downstream of the outflow boundary, therefore the static pressure is specified. This pressure is specified using the natural boundary condition on the momentum equation. All other flow quantities are unspecified.

Slip Wall

A slip wall is obtained by setting the normal velocity $\boldsymbol{V}\cdot\boldsymbol{n}$ equal to zero and setting the tangential surface traction equal to zero. The density is unspecified, and the normal heat flux is set to zero. This boundary condition is also used to model a plane of symmetry.

No-Slip Wall

No-slip walls can be one of two types, either specified heat flux walls (including adiabatic walls) or specified temperature walls. For a specified heat flux wall, the heat flux is added using the natural boundary condition on the energy equation. A constant temperature wall is obtained using a constraint on the total energy. For either of these cases, the u and v components of velocity are set to zero, and the density is unspecified.

The boundary condition for the solid conservation of energy equation is either specified temperature or specified heat flux. The temperature for the solid is a primary unknown, so a specified temperature boundary condition is trivial. A specified heat flux boundary is obtained using the natural boundary condition.

Applications

The following problems were analyzed using the present algorithm. Although the algorithm allows for a general equation of state for the fluid, a perfect gas has been assumed in the present applications. Triangular elements were used in all calculations, and linear interpolation functions were used for the conservation variables and fluxes. The value of θ was set to 1 for all of the applications, and the convergence criteria was a reduction in the residuals of the conservation variables from one time step to the next of greater than five orders of magnitude. Further applications using the present algorithm can be found in Ref. 12.

Backward-Facing Step

To test the flow algorithm for low speed flow, a two-dimensional problem was chosen where a fully developed internal flow expands over a backward-facing step. The problem statement and channel configuration are illustrated in Fig. 2. Flow separation occurs at the leading edge of the step, and primary, secondary, and even tertiary recirculation regions develop depending on the Reynolds number of the incoming flow. The boundary conditions used for this problem are a fully developed (parabolic) velocity profile and uniform den-

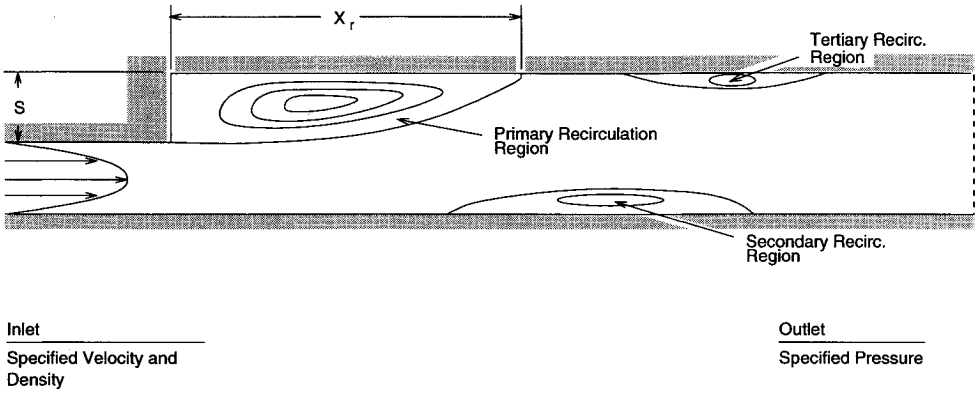

Fig. 2 Problem statement for backward-facing step flow.

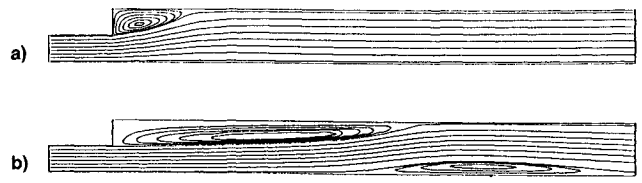

Fig. 3 Streamlines for backward-facing step flow. Re = a) 100 and b) 800.

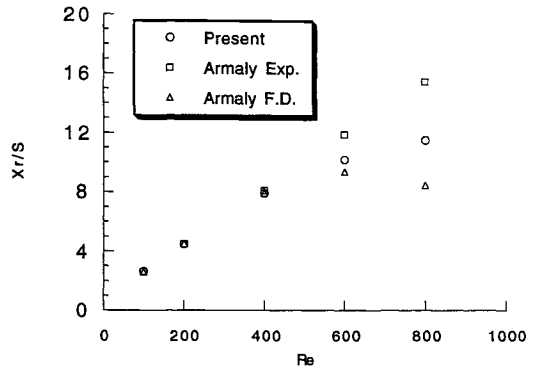

Fig. 4 Reattachment length vs Reynolds number for backward-facing step flow.

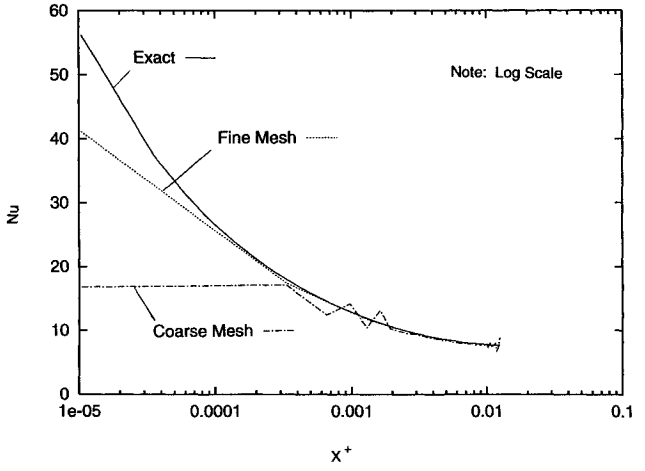

Fig. 5 Local Nusselt number for thermally developing flow.

sity profile on the inflow plane, no-slip adiabatic walls, and a subsonic outflow plane where the static pressure is specified. The computational mesh, containing 4877 elements, is unstructured and clustered in the vicinity of the step.

An extensive study of this problem was carried out both experimentally and numerically by Armaly et al.[13] According to Armaly, for $Re \leq 400$, only the primary recirculation region is present. For $Re > 400$, however, a secondary recirculation region begins to form on the wall opposite the step due to the adverse pressure gradient caused by the sudden expansion. As this region begins to form, according to Armaly's experimental observations, the flow becomes three-dimensional in nature, and the assumptions of two-dimensional flow are no longer valid.

The flow was analyzed with the present algorithm assuming a variable density flow even though the Mach number was on the order of 1×10^{-3}. The computational results show, as expected, that the density changes are extremely small, and that this flow could be analyzed with other algorithms assuming constant density. Plots of streamlines for Reynolds numbers of 100 and 800 are shown in Fig. 3. Because of the three-dimensional nature of the flow for $Re > 400$, the results for $Re = 800$ are not expected to be accurate, but the streamlines are shown for this Reynolds number to demonstrate the ability of the present algorithm to predict the primary and the secondary recirculation regions described by Armaly.

The problem was solved using the current algorithm for $100 < Re < 800$ and compared with Armaly's numerical and experimental results. The reattachment length of the primary recirculation region X_r (see Fig. 2) is plotted as a function of the Reynolds number in Fig. 4. The reattached length was determined by examining the signs of the velocity a small distance away from the wall. The numerical solutions obtained with the present algorithm are in excellent agreement with the experimental and numerical results of Armaly for $Re \leq 400$. For larger Reynolds numbers, however, the numerical results obtained with both the present algorithm and Armaly's finite difference algorithm (also a two-dimensional algorithm) begin to disagree with the experimental results. This is presumably due to the three-dimensional nature of the flow for $Re > 400$.

Thermally Developing Flow (Graetz Problem)

The main purpose of the current algorithm is to solve problems of steady-state convective heat transfer. The case of a thermal boundary layer developing within a hydrodynamically fully developed flow is one of the few examples of this type of problem where a closed form analytical solution is available. The problem consists of flow between parallel plates subjected to either uniform heating or specified wall temperature. The velocity field of the fluid is considered uniform in the flow direction and known throughout the channel. The velocity profile can be either constant (slug flow) or parabolic (fully developed viscous flow).

The current algorithm was used to solve this problem using a prescribed wall temperature. While the velocity profile is expected to be constant along the length of the channel, the current method was used to solve for both the velocity field and the temperatures. On the inflow plane, the u velocity was specified with a parabolic profile, the v velocity was specified as zero, and the density was specified with a uniform profile. Since this problem is symmetric about the centerline of the channel, only the upper half of the channel was analyzed. The lower boundary was treated as a plane of symmetry, whereas the upper boundary was treated as a no-slip specified temperature wall. The outflow plane was treated as a subsonic outflow, with specified static pressure.

The problem was solved on two different meshes to study the effects of mesh size on heat transfer results. The coarse mesh had 60 nodal points along the upper wall, whereas the fine mesh had 240. Both meshes were clustered in the vicinity of the thermal leading edge to capture the steep temperature gradients in this region. The results in terms of the Nusselt number obtained on both meshes are plotted in Fig. 5. The nondimensional length x^+ is defined by $x^+ = 2x/(D_h RePr)$ where Re is based on the hydraulic diameter (D_h = twice the channel height h). Using this nondimensionalization, Brown[14] presented an infinite series analytical solution to this problem that is used for comparison to the current results. In the analytical solution, the Nusselt number goes to infinity asymptotically as x^+ approaches zero, so the computational results obtained on both meshes diverge from the exact solution for x^+ less than about 0.001. The results obtained on the coarse mesh however, demonstrate substantial oscillations of the Nusselt number for $x^+ \leq 0.002$. These oscillations are presumably due to a lack of mesh resolution. Nonphysical spatial oscillations of flow quantities, such as those appearing in Fig. 5, are typical of results obtained using Galerkin discretization techniques with no artificial diffusion such as the current algorithm. Oscillations of this nature can be eliminated by mesh refinement as demonstrated by the fine mesh results in Fig. 5.

The results for this problem demonstrate: 1) the ability of the current algorithm to accurately predict heat transfer for a simple low-speed flow; and 2) the nonphysical spatial os-

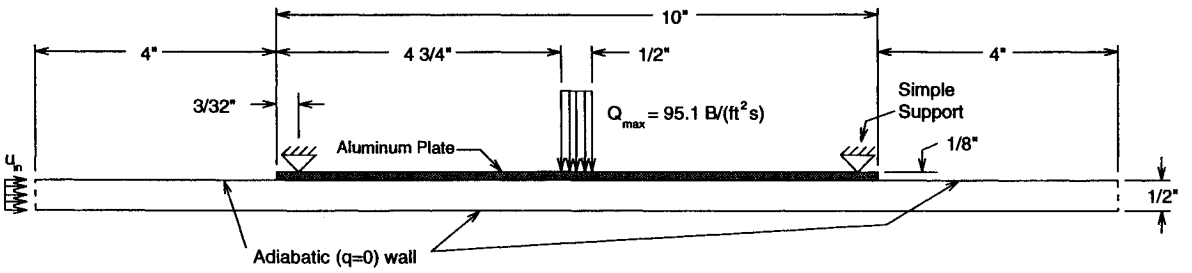

* The plate has insulated ends and upper surface.

Inlet Conditions:	Outlet Conditions	Initial Conditions
Specified:	Specified:	Fluid:
$u = u_{in}$	P = 3.0 psig	Uniform $u = u_{in}$, v = 0
v = 0	Unspecified:	Density = 0.08731 lbm/ft^3
Density	Density, u, v	$T = 80^0$ F
Unspecified:		Solid:
Total Energy		Uniform $T = 80^0$ F

Fig. 6 Problem statement for convectively cooled plate computational model.

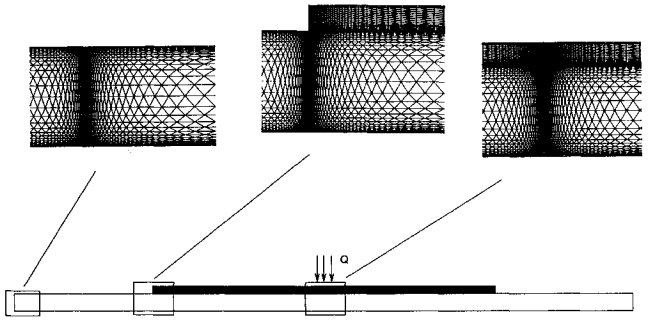

Fig. 7 Computational mesh for convectively cooled plate.

cillations that can result when using the current algorithm with an insufficient mesh.

Convectively Cooled Plate

Research is currently being conducted to understand the fluid-thermal-structural interaction of convectively cooled structures subjected to substantial, localized heat loads. An experimental setup is under construction to investigate structures of this type. The purposes of the experiment are to test the response of convectively cooled plates at high temperatures and to study the flow-thermal-structural interaction between a hot, deforming plate and a coolant flow. An initial analysis was performed for this experimental setup using the current algorithm.

The experimental setup consists of a closed loop of air that flows past a plate subjected to an intense heat flux. The flow driven by a compressor is straightened and cooled to a controlled temperature, then flows through a test section where the fixed panel is heated. The conditions in the test section can be in the range of 0–9 psig for the pressure, and 0–100 ft/s for the inlet air velocity. The heating is provided by a quartz heat lamp capable of producing heat fluxes of up to 95.1 Btu/ft^2-s over a $\frac{1}{2}$-in.-wide strip.

The experimental test section is modeled numerically as a two-dimensional flow in the x-y plane. The inlet air is treated as an ideal gas at T = 80°F and P = 3.0 psig. The problem statement for the numerical model is illustrated in Fig. 6. The flow inlet plane is treated as a subsonic inflow boundary with the density and velocity specified with constant profiles. The outflow plane is treated as a subsonic outflow with a specified pressure of 3.0 psig. The walls of the channel are all treated as insulated no-slip wall boundaries with the exception of the interface between the solid and the fluid. The plate material used in the current study is $\frac{1}{8}$-in.-thick aluminum alloy (2024-T6) with a thermal conductivity of 106.7 Btu/(h·ft·R). The thermal conductivity of the solid is held constant throughout the analysis. The ends and entire upper surface of the plate are insulated except in the region of the applied heat flux. The applied heat flux in the present example is equal to 10% of the maximum heat output of the lamp (9.51 Btu/ft^2-s). The initial conditions of the fluid are constant and equal to the inflow plane except at the no-slip walls where the velocity goes to zero. The plate initially has a uniform temperature of 80°F.

The fluid mesh used to model this experiment contains 8728 nodes and 16,864 triangular elements. This mesh is concentrated heavily in the regions where intense temperature and velocity gradients are expected, such as in the vicinity of the applied heat flux, the leading edge of the channel, and the leading and trailing edges of the plate. The inlet air velocity used is 25 ft/s. This inlet velocity gives a Reynolds number based on hydraulic diameter of approximately 14,500. Because the Reynolds number used in this study is relatively high, the boundary layers (both thermal and hydrodynamic) are very thin, and the mesh is graded so that it is very fine close to the wall throughout the mesh to capture the velocity and temperature gradients associated with a thin boundary layer. The solid mesh contains 2900 nodes and 5472 elements. The mesh used to model the fluid and plate is shown in Fig. 7.

Temperature and density cross-sectional profiles at various x locations along the length of the channel are shown in Figs. 8 and 9, respectively. Figure 8 also includes the temperature profiles through the thickness of the plate. Figure 8 reveals substantial temperature gradients in the fluid near the wall, but because the solid material has a high thermal conductivity, the temperature gradients through the thickness of the solid are very slight. Substantial density gradients through the channel can be seen in Fig. 9. The maximum change in density across the flow channel occurs at the x location of the input heat pulse, and is approximately 47%.

A primary parameter of interest in the study of thermally induced plate deformation is the variation of the temperature along the length of the plate. Intense spatial temperature gradients in plates induce high compressive stresses leading to significant out of plane buckling. A plot of temperature along the length of the plate for the present study is shown in Fig. 10. The length S used for normalization in this and all following figures is the length of the plate. This figure illustrates that the input heat is well distributed along the length of the plate due to its high thermal conductivity. The maximum temperature difference along the plate for this case is about 176°F.

The final analysis performed is an initial study of the effects of plate deformation on convective cooling. The same $\frac{1}{8}$-in.-thick aluminum plate is given the deflected shape of a simply

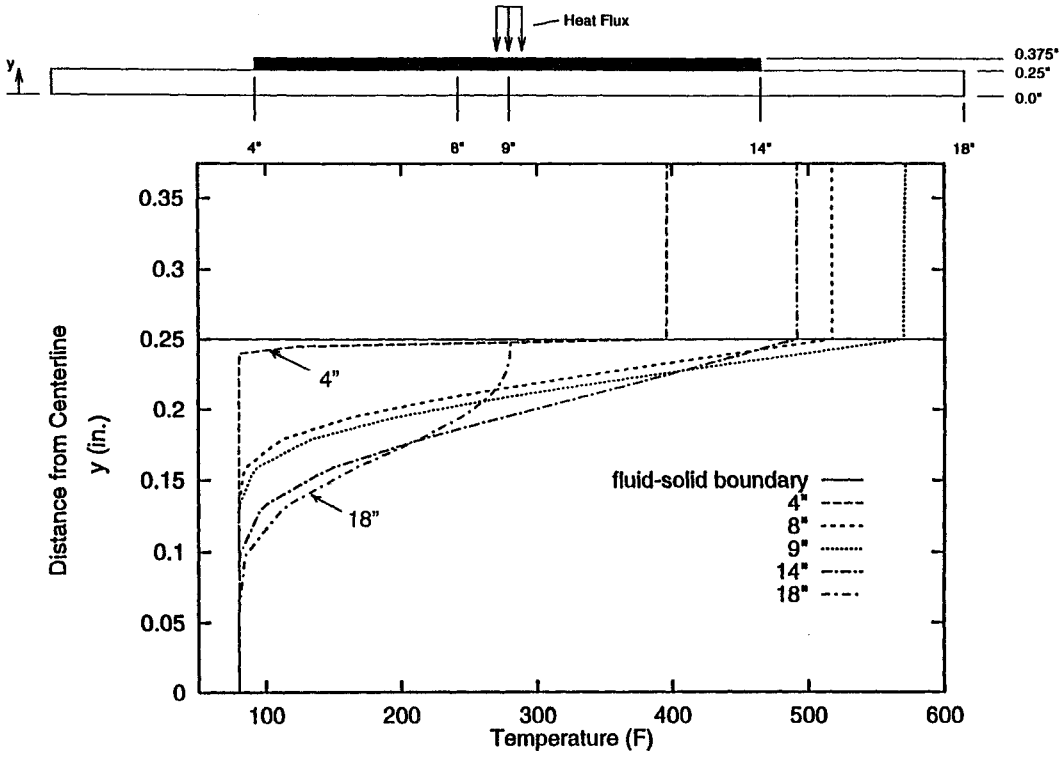

Fig. 8 Cross-sectional temperature profiles for convectively cooled plate.

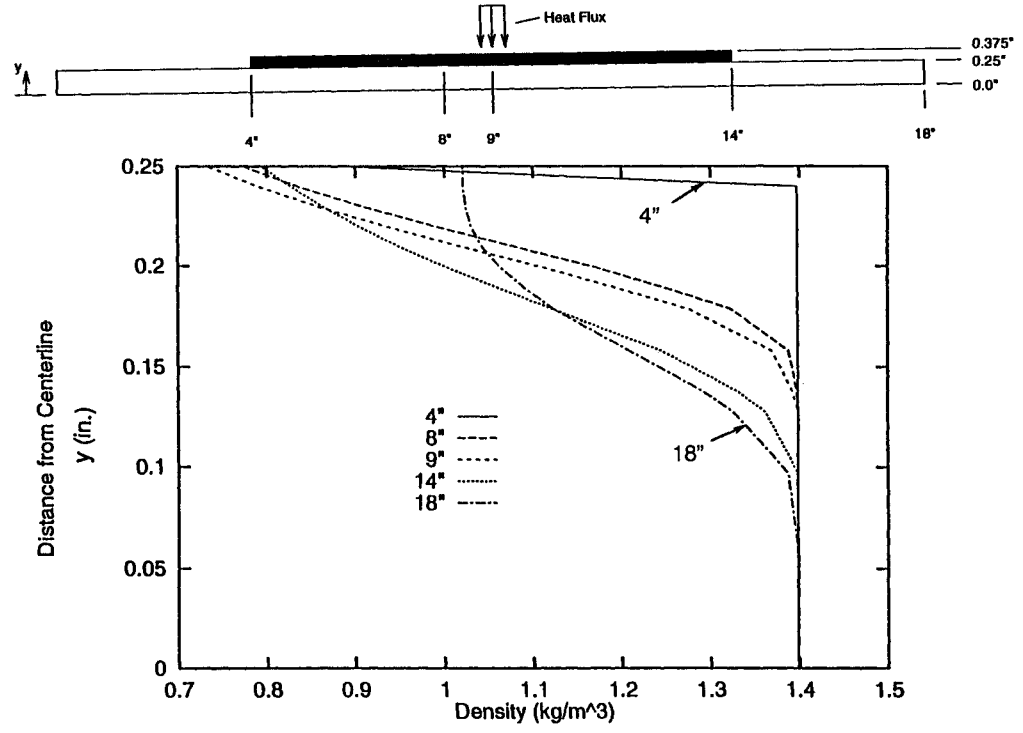

Fig. 9 Cross-sectional density profiles for convectively cooled plate.

supported beam subjected to uniform pressure loading. The maximum plate deflection is specified to be one plate thickness at the centerline. All fluid and solid boundary and initial conditions are identical to the previous case of a straight channel. The computational mesh used to analyze the new geometry is also the same, but the node locations have been moved to reflect the plate deformation.

The analysis was done for the channel using two different mass flow rates to demonstrate that the plate deformation affects the heat transfer characteristics differently depending on the flow rate. The two inlet velocities used were 6.25 and 37.5 ft/s. For each of these flow rates, results of temperature along the fluid-solid interface are plotted in Fig. 11 for both a deformed plate analysis and an undeformed plate analysis. The temperature of the plate increases for the deformed plate in both cases because the flow decelerates under the plate to accommodate the increased flow area. An interesting feature to note is that not only are the temperature plots substantially different for the deformed and undeformed plates at each velocity, but also that as the velocity of the flow increases, the differences between the two results become more pronounced. This is because as the velocity in the channel in-

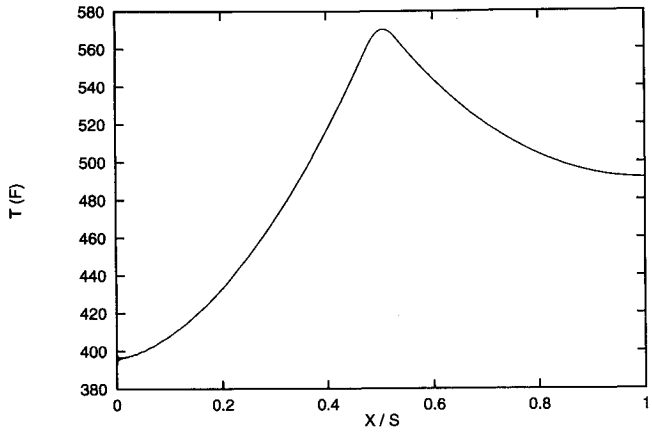

Fig. 10 Temperature at fluid-solid interface for convectively cooled plate.

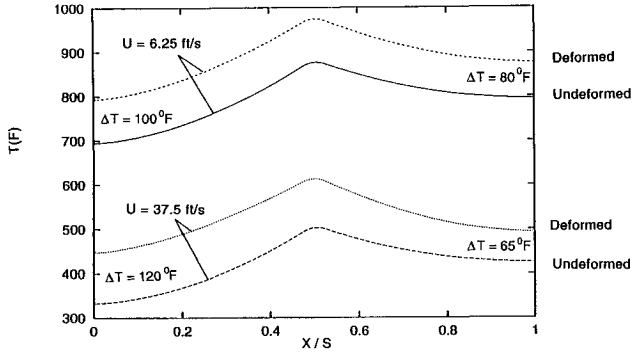

Fig. 11 Temperature at fluid-solid interface for deformed vs undeformed plate.

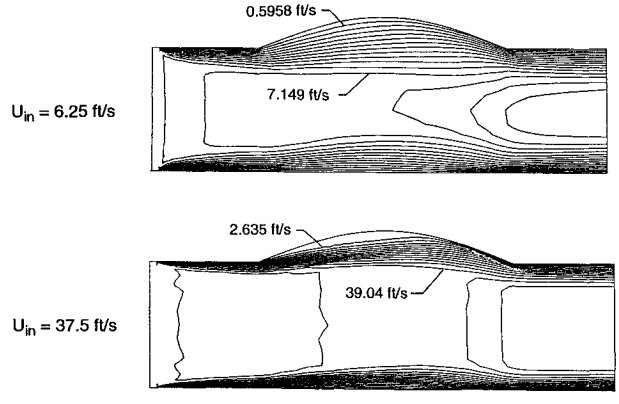

Fig. 12 Velocity contours for deformed convectively cooled plate.

creases, the flow rate near the wall behind the plate leading edge slows due to an increasing strength adverse pressure gradient. In other words, a recirculation region is beginning to form behind the plate leading edge.

To illustrate the flow recirculation region, contours of u velocity are shown in Fig. 12 for both inlet velocity cases. Note on these plots that the y axis has been stretched so that the contours can more easily be seen. The velocity contours for the faster flow rate clearly show a pocket of very slow flow that occurs behind the leading edge. The recirculation region in the faster flow rate case has two effects. First, because the velocity near the wall behind the leading edge of the plate is small, the effectiveness of the convective heat transfer mechanism is reduced. Second, because the fluid in this region is hotter farther from the plate, the density will be lower and the heat capacity of the fluid in this region is reduced. The combination of these two effects tend to insulate the plate in this region and the difference in temperatures between the deformed and undeformed cases is greater. On the other hand, toward the plate trailing edge, the velocity near the plate is increasing, which enhances the heat transfer, so that the difference in temperature between the deformed and undeformed plates is smaller than at the plate leading edge. For the slower inlet velocity case, there is very little difference between the velocity near the plate at the leading and trailing edge, so the difference in temperatures between the deformed and undeformed plate cases are nearly uniform over the length of the plate.

Concluding Remarks

A Galerkin-based algorithm for simultaneously solving the equations governing convection and conduction heat transfer is presented for analyzing forced convection flows within convectively cooled structures. The compressible form of the flow equations are used to accurately represent gradients of density and other flow quantities that accompany intense temperature gradients. The algorithm is implemented as a transient scheme that may be either implicit or explicit.

The algorithm is used to analyze several problems involving low-speed flow. Two problems chosen have small Mach numbers and relatively small temperature gradients to compare with well-documented incompressible flow solutions. The solutions for these problems demonstrate that the algorithm performs well when applied to low-speed flows with relatively constant properties.

The algorithm is then used to analyze an experimental model of a convectively cooled structure. This experiment consists of flow in a channel bounded by a solid plate subjected to an intense local heat flux. The algorithm is first used to analyze a straight channel configuration. Anticipating the plate deformation caused by spatial temperature gradients, an initial study of the effects of plate deformation on convection heat transfer is then performed. It is found that even a small out of plane deformation of the plate causes a substantial difference in plate temperature results, and that the differences are intensified as the velocity of the fluid increases.

Acknowledgments

The authors would like to thank Allan R. Wieting, Head, Aerothermal Loads Branch, NASA LaRC for his support of this work as technical advisor. The first author began this work as a graduate research assistant at the University of Virginia and continued it as an associate engineer working for Lockheed Engineering & Sciences Company (LESC) under the support of a NASA contract NAS1-19000. The authors would also like to thank Kim Bey of the Aerothermal Loads Branch for very helpful technical discussions.

References

[1]Shore, C. P., "Review of Convectively Cooled Structures for Hypersonic Flight," Society of Automotive Engineers Aerospace Vehicle Technology Conf., May 1986 (NASA TM-87740).

[2]Wieting, A. R., "Multiple Shock-Shock Interference on a Cylindrical Leading Edge," *AIAA Journal*, Vol. 30, No. 8, 1992, pp. 2073–2079.

[3]Thornton, E. A., Oden, J. T., Tworzydlo, W. W., and Youn, S. K., "Thermoviscoplastic Analysis of Hypersonic Structures Subjected to Severe Aerodynamic Heating," *Journal of Aircraft*, Vol. 27, No. 9, 1990, pp. 826–835.

[4]Thornton, E. A., and Wieting, A. R., "Finite Element Thermal Analysis of Convectively Cooled Aircraft Structures," *Numerical Methods in Heat Transfer*, edited by R. W. Lewis, K. Morgan, and O. C. Zienkiewicz, Wiley, New York, 1981, pp. 431–443.

[5]Patankar, S. V., "Recent Developments in Computational Heat Transfer," *Journal of Heat Transfer*, Vol. 110, Nov. 1988, pp. 1037–1045.

[6]Scotti, S. J., "Numerical Studies of Convective Cooling for a Locally Heated Skin," NASA TP-3100, May 1991.

[7]Carlisle, R. G., and Wood, H. G., III, "Computational Study of Coolant Flow of Liquid Hydrogen Through an Externally Heated Duct," *Journal of Thermophysics and Heat Transfer*, Vol. 7, No. 3, 1993, pp. 418–425.

[8]Ramakrishnan, R., Bey, K. S., and Thornton, E. A., "Adaptive Quadrilateral and Triangular Finite Element Scheme for Compressible Flows," *AIAA Journal*, Vol. 28, No. 1, 1990, pp. 51–59.

[9]Thornton, E. A., and Dechaumphai, P., "Coupled Flow, Thermal and Structural Analyses of Aerodynamically Heated Panels," *Journal of Aircraft*, Vol. 25, No. 11, 1988, pp. 1052–1059.

[10]Dechaumphai, P., "Evaluation of an Adaptive Unstructured Remeshing Technique for Integrated Fluid-Thermal-Structural Analysis," *Journal of Thermophysics and Heat Transfer*, Vol. 5, No. 4, 1991, pp. 599–606.

[11]Huebner, K. H., and Thornton, E. A., *The Finite Element Method for Engineers*, Wiley, New York, 1982, pp. 292, 293.

[12]Yarrington, P. W., "Finite Element Analysis of Low-Speed Compressible Flows Within Convectively Cooled Structures," M.S. Thesis, Univ. of Virginia, Charlottesville, VA, May 1993.

[13]Armaly, B. F., Durst, F., Pereira, J. C. F., and Schönung, B., "Experimental and Theoretical Investigation of Backward-Facing Step Flow," *Journal of Fluid Mechanics*, Vol. 127, 1983, pp. 473–496.

[14]Brown, G. M., "Heat or Mass Transfer in a Fluid in Laminar Flow in a Circular or Flat Conduit," *AIChE Journal*, Vol. 6, 1960, pp. 179–183.